FEM-simulation of gas diffusion in solid closed-cell porous materials

Alexander Rassloff, Sascha Heitkam, Gaetan Dalongeville, Christian Gauthier, Thierry Roland

FEM-Simulation of Gas Diffusion in Solid Closed-Cell Porous Materials

Alexander Raßloff[a,c], Sascha Heitkam[b], Gaëtan Dalongeville[c], Christian Gauthier[c], Thierry Roland[c,*]

[a] *Faculty of Mechanical Science and Engineering, Technische Universität Dresden, 01069 Dresden, Germany*
[b] *Institute of Fluid Dynamics, Helmholtz-Zentrum Dresden-Rossendorf, Bautzner Landstraße 400, 01328 Dresden, Germany*
[c] *Institut Charles Sadron, C.N.R.S, Université de Strasbourg, rue du Loess, B.P. 84047, 67034 Strasbourg cedex 2, France*

Abstract

The past decades witnessed growing interest in polymeric closed-cell porous materials. They are lightweight, robust and find applications in many different sectors, like packaging, thermal insulation or cushioning. Numerical simulations are commonly used in the construction process to predict the behaviour of the products in application. So far, gas diffusion has often been neglected, as there are no tools available to include it. Therefore, this paper aims to present an algorithm to include the simulation of gas diffusion into a commercial finite element analysis (FEA) tool, at the example of *MSC Marc*. Using the similarity of thermal conductivity and gas diffusion, the thermal solver of the FEA program is exploited to perform the simulation of gas diffusion. Some first two-dimensional numerical simulations of porous closed-cell models under long-term load show promising results. Effective diffusion coefficients are obtained and conclusions about the time scale are made. The results agree to analytical estimations of the diffusion process. A notable influence of gas diffusion on long-term loaded porous materials can be shown.

Keywords: Gas diffusion, Void material, Numerical simulation, Finite element method, Gas diffusion coefficient

1. Introduction

Solid foams and other porous closed-cell structures are of great interest in engineering [1]. They are lightweight, insulating and shock-absorbing. The advancement in production techniques paves the way to new structures and geometries. For this reason, understanding porous materials' properties and applications is of significant interest. The objective of this paper is to provide a method for the simulation of gas diffusion in closed-cell porous material under mechanical load and to document first findings. Within this work, all materials are considered to contain only closed pores or cells. This gas diffusion phenomenon has been experimentally shown in several polymeric natures of foams, among them polypropylene foams [2]. In this work, using specific compression tests in a fluid chamber, Bouix et al. pointed up a progressive and slow gas

*Corresponding author
Email addresses: alexander.rassloff@tu-dresden.de (Alexander Raßloff[a,]), s.heitkam@hzdr.de (Sascha Heitkam), christian.gauthier@ics-cnrs.unistra.fr (Christian Gauthier), thierry.roland@ics-cnrs.unistra.fr (Thierry Roland)

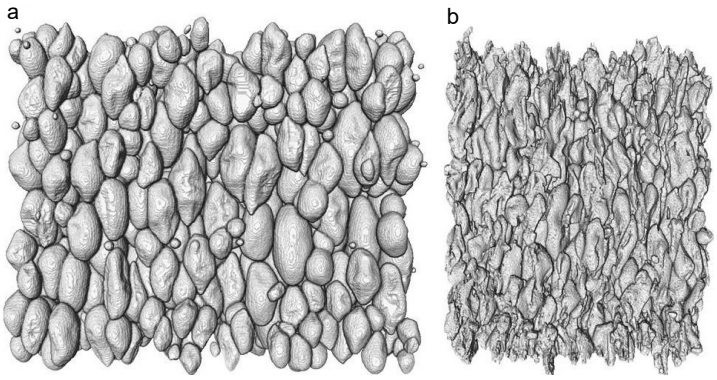

Figure 1: Closed-cell foam observed at atmospheric pressure using X-ray tomography. Initial state (a) and collapse configuration once gas escaped by diffusion (b). A reduction by about 50% is observed in width and 7% in height. Thick polymeric skin present at the top and bottom of the sample may explain the difference in the size reduction regarding the direction.

escapes during the whole deformation process of foams subjected to quasi-static compression. In the same manner, putting a closed-cell foam in a reduced environmental pressure we showed by X-ray tomographic reconstruction a tendency for the pore structure to collapse as gas diffuse out. Figure 1 is an illustration of the evolution of the structure. It shows on the left side the initial state of the thermoplastic closed-cell foam and on the right one the collapse configuration as pores are empty of gas and experience ambient pressure. This demonstrates how diffusion can be related to problem of dimensional stability during storage of foam or semifoam product. Also, this diffusivity process may be quite fast. For instance, the PU foam blown with CO_2 shows some shrinkage within two months after its production as a significant reduction of the pore pressure is attained [3].

Knowing about the degassing behaviour of porous materials, especially about the time scale, is of major importance to industry as the lifetime of such products is strongly related to it. Elasticity and insulation properties depend on the kind and amount of gas contained in the material's pores. Also, since several blowing agents are about to phased out under recent international regulations for chemical uses (REACH), understanding how different gases affect the ageing behaviour is a prerequisite for the development of foam with alternative CBA. Thermal insulation boxes lose rigidity and their insulation properties with time, especially under load, when filled with ice, fish or heavy content, as the gas diffuses out of the pores. The same applies to foam sealing, cushioning and many more applications, where porous materials, such as foams, are exposed to long-term loads. In industrial packaging foam-like materials are used to absorb shocks to protect the packed content. Hereby, the absorption behaviour is mainly determined by the amount of gas stored in the wrap or fill material [4]. The following equation relates the collapse stress to the relative density [1]:

$$\frac{\sigma^*_{\mathrm{pl}}}{\sigma_{\mathrm{pl}}} = 0.3 \left(\phi \frac{\rho^*}{\rho} \right)^{1.5} + 0.4 \left(1 - \phi \right) \left(\frac{\rho^*}{\rho} \right) \tag{1}$$

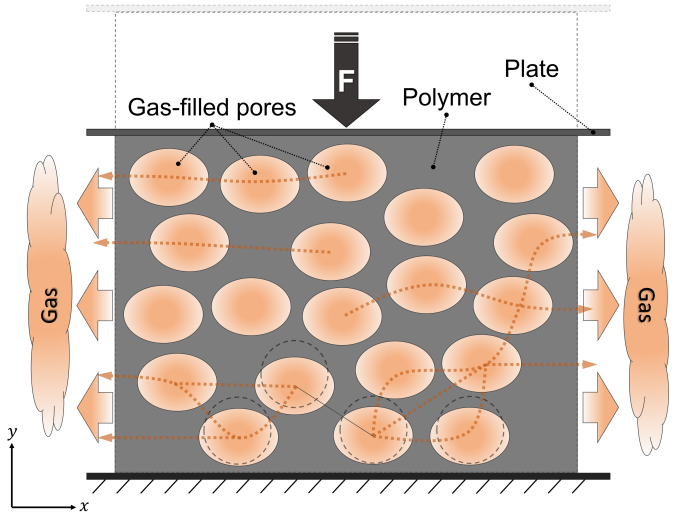

Figure 2: Basic set-up: Deformed two-dimensional porous material between two plates under compressive force F. Gas diffuses through pores and bulk material (polymer) to both sides (left and right).

where σ^*_{pl} is the collapse stress of the foam, σ_{pl} the one of the solid material, ϕ the volume fraction of cell edges in a unit volume and $(1-\phi)$ the remaining fraction of the solid contained in the pore faces, ϕ^* the density of the foam and ϕ the density of the solid material. Considering this equation (1), it was shown that compression at low strain rate leads to plateau stress data lying close to line for $\phi = 1$. This suggests that pores deform primarily through plastic buckling and bending of their edges. However, for high strain rate, collapse stress comes closer to the linear term of the equation (line for $\phi = 0$) which refers to compression and stretching of the pore faces. This apparent higher contribution of the pore faces is mainly due to inertia effects and to the fact that gas bubbles cannot escape from the foam due to the short time. Therefore, the foam strength increases during dynamic loading because of the entrapped gas in the closed pores. As a constantly high absorption level is demanded, there should be no or low change regarding the properties of this material, i.e. negligible gas diffusion.

Thus, gas diffusion is a major issue for several applications. To provide reliable and realistic behaviour laws there is a need for a temporal analysis taking into account both mechanics and gas diffusion. This problematic concerns polymer foams but beyond that others materials as cork stoppers for which oxygen transfer across the pore walls was demonstrated to follow a Fickian mechanism [5].

However, comparatively few attempts have been made to numerically simulate gas diffusion in realistic porous materials. Previous research concentrated on theoretical models to predict effective diffusion coefficients. Alsoy [3] compares existing approaches for this calculation for closed-cell polymeric foams. She makes comparisons between their theoretical predictions and experimental values. An algorithm for a one-dimensional simulation of pore concentration change due to diffusion is presented, relying on several as-

sumptions. It requires a network of cubic pores with constant wall thickness, i. e. uniform and constant pore sizes, a homogeneous and isotropic foam and diffusion in only one direction. Pilon et al. [6] present, likewise on the idea of a cubic unit cell model, an engineering model to predict diffusion coefficients in closed-cell foams. Briscoe and Savvas [7] use elastic models with springs and arrays of rectangular pores in a row for the prediction. The idea of the application of the Finite Element Method (FEM) to simulate Fickian mass transport was mentioned by Wadiak [8]. This work shows the usage for a multi-layered polymeric body with no porosity. Nonetheless, it introduced the idea to use existing and effective thermal solvers for diffusion problems. Many projects focus on an experimental approach [9, 10, 11, 12] to calculate diffusion coefficients or to investigate gas pressure changes in porous materials.

So far, prior theoretical research was limited to fixed geometries with approximations of wall thickness and areas. It has neglected to provide insight into the diffusion process going on in the material. There are no methods documented that consider directly the interaction between mechanical deformation of the porous material and the diffusion process, especially under changing loads. Therefore, a method is presented to integrate gas diffusion processes into structural mechanic FEM simulations. It allows arbitrary geometries and gas diffusion in three dimensions, is not limited to high foam-porosities and can calculate the process under different, time-dependent load-scenarios. Embedded in a commercial FEA program, MSC Marc, it is comfortable and efficient to use. Major advantage of the present numerical model is the possibility to evaluate the effect of foam structure (pore wall thickness, pore size, porosity distribution, topological arrangement) and possible anisotropic pore shape (often met with industrial foam). But also, to quickly take into account the influence of the polymer material constitutive laws by which we may implicitly reflect different physical states of the material as changes of crystallinity or cross-linking.

Using the analogy between Fickian diffusion and thermal conduction, the thermal solver of the FEA software is used to simulate the diffusion. Due to deformation of the pores and due to gas diffusion, the pore pressures change. In a parallel approach, both are calculated and accumulated for each time step. By this, gas pressure and stress distributions throughout the whole domain are obtained for every time step. Post-processing allows the extraction of characteristic values, e.g. an effective diffusion coefficient. The method is implemented to simulate two-dimensional configurations under constant load as depicted in figure 2. In particular, the effect of geometrical pore shape on both the ageing profile and the effective diffusion coefficient is discussed based on results from the simulation. When closed-cell foams are produced by expansion, usually at high strain rate, pore elongation is induced in one direction which may results in anisotropic effect of the mass transfer in the polymer.

2. Methods

2.1. Theory of Gas Diffusion in Solid Closed-Cell Porous Materials

Gas diffusion describes the transport of gas in gas, liquid or solid due to the Brownian motion of gas molecules. It is a process in which gas passes from locations of higher concentration to ones of lower concentration. If the locations are separated by a solid, the gas needs to permeate it and diffuse through this material. Diffusion through condensed matter depends on the concerning material, the permeating gas, and on the temperature. Polymers are a group of materials where gas diffusion is relatively fast. Free volume that arises from the gaps left between entangled polymer chains is responsible for this aspect and usually a good correlation is found between diffusion rate and the degree of the macromolecular chains flexibility. Indeed any external force field acting on the molecular chain mobility has an important effect by opening or closing pathways for diffusion. Boersma et al. [13] studied the effects of tensile stress applied to plastic films on their oxygen permeation properties and reported an increase in permeation rate with stress. Nonetheless, it can often be neglected for most non-porous materials upon a certain thickness. Gas diffusion in gases is usually several orders of magnitudes faster than diffusion in solids or liquids. Thus, the time scale for diffusion is usually determined by the way gas diffuses through the pore wall. Gas diffusion as consequence of transient chemical bonding is not considered for this paper on solid closed-cell materials.

The basis for all models is *Fick's law of diffusion*

$$J = -D\nabla c \tag{2}$$

with J the flux of gas mass, c the concentration of gas and D the diffusion coefficient. By taking the mass-balance into account Fick's first law of diffusion can be transferred to the fundamental differential equation of diffusion or *Fick's second law of diffusion*

$$\frac{\partial c}{\partial t} = D\nabla^2 c. \tag{3}$$

In this work, it is assumed that the diffusion coefficient D in the solid material is constant, i. e. independent of the local gas concentration and mechanical stress in the solid material. Gas diffusion inside the pores is considered to be infinitely high, yielding homogeneous pressure and concentration inside each pore. For this work, the gaseous environment is considered to consist of a single gas.

The derivation of an analytical solution $c(\vec{x}, t)$ of this differential equation for complex boundary conditions is not feasible. For this reason, several models for the prediction of effective diffusion coefficients have been developed as mentioned above. We are not aware of any study that simulates complex structures under mechanical load to gain insight into diffusion *in* porous materials. Nonetheless, prior research helps to understand the basic mechanism that needs to be modelled.

The foam or porous material has either due to its production or due to an external load a higher pressure in its pores than ambient pressure. This causes a concentration imbalance because gas pressure

and concentration are linked. In the present study (above the glass transition temperature), *Henry's law* is applied for this relation

$$c = S \cdot p \tag{4}$$

with S being the solubility of the gas in the solid material S_s or in the pore S_p and p the local gas pressure. Due to the pressure gradients, the gas diffuses through the walls of the porous solid. By this, it evokes a change of pressure in the pores until an equilibrium is reached. The solubility in pore and solid is considered to be constant. Here, the polymer is considered to be in its rubbery state. It is generally agreed that the solubility depends neither on the gas concentration nor on the hydrostatic pressure applied to the polymer [14, 15]. Also, for a wide range of temperature, it appears that variations of the solubility coefficient are less important than variations of the diffusion coefficient. Thus, the variations of D mainly affect the values of the permeability.

2.2. Set-up

The two-dimensional model for the numerical simulation is illustrated in figure 2. A block of porous material with a certain width w, height h and porosity ϕ is subjected to a vertical, mechanical load p_load.

Either spherical or elliptical pores of equal volume are arranged either on a Cartesian lattice or are randomly distributed. Pores are well separated from each other and from the boundaries to diminish possible distortion of the meshed domains.

Figure 3 illustrates the boundary and initial conditions applied on the material as collected in table 1. At the top boundary, the integral normal force F_load is prescribed on a rigid plate, leading to a time-dependent and homogeneous normal displacement of the top boundary. Tangential stress at each node of the top boundary is set to zero. At the bottom boundary, zero normal displacement and zero tangential stress is prescribed by using a rigid plate with fixed displacement. No gas diffusion is allowed at the top and bottom boundary. At the side boundaries, the ambient pressure is applied as a normal mechanical load and tangential load is set to zero.

Table 1: Boundary and initial conditions

Boundary Condition	Top	Bottom	Left/right	Pore
Normal displ.	free, same for whole area	zero	free	free
Normal stress	$F(t)$	free	ambient pressure	pore pressure
Tangent. disp.	free	free	free	free
Tangent. stress	zero	zero	zero	zero
Gas pressure	zero gradient	zero gradient	const ambient pressure	const for each pore

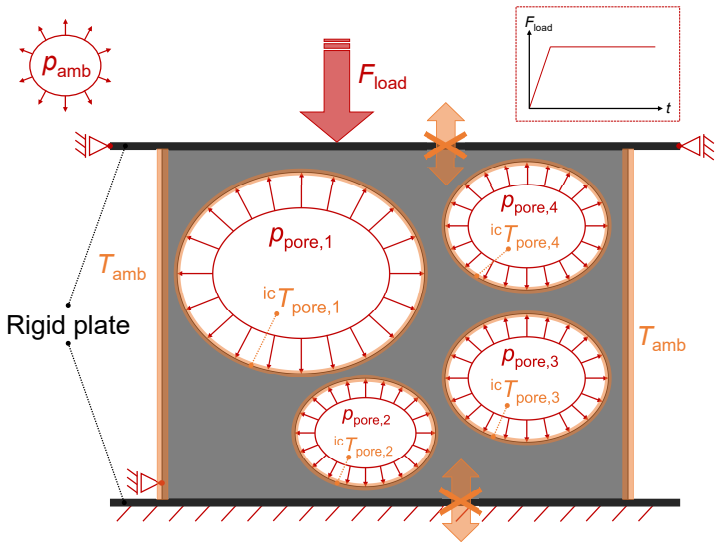

Figure 3: Boundary and initial conditions. *Mechanical boundary conditions:* Two-dimensional closed-cell porous material subjected to compressive force F_{load}. Material is compressed in between to rigid plates, of which the bottom one is fixed in displacement and the top one fixed in normal displacement. A mechanical pressure $p_{\mathrm{pore},i}$ is acting on pore i. Mechanical ambient pressure p_{amb} acting on both sides. *Diffusion/temperature boundary conditions:* Ambient pseudo-temperature T_{amb} applied to the sides. Zero flux over the top and bottom boundary. Initial pseudo-temperature ${}^{\mathrm{ic}}T_{\mathrm{pore},i}$ applied to pore i.

Dimensional quantities are used for the simulations as collected in table 2. They are chosen to represent typical structures and do not resemble any particular porous material. Triangular finite elements of first order (linear – 3 nodes) are used for the simulations.

2.3. Numerical Method

Fourier's law of thermal conduction and *Fick's law* share the same structure. Wadiak [8] proposed in 1985 to adapt existing FEM code to solve Fickian mass transport through polymers. Thermal conduction is already implemented in many FEA programs, so in MSC Marc. Exploiting the thermal solver for simulating gas diffusion is the idea behind this approach. For this purpose, both equations are compared, and the quantities of the mass transport are expressed in quantities of Fourier's law.

Assuming constant density ρ, constant specific heat capacity c_{p} and constant thermal conductivity k, as well as no thermal sources, the *law of thermal conduction* denotes

$$\frac{\partial T}{\partial t} = \frac{k}{\rho c_{\mathrm{p}}} \nabla^2 T \tag{5}$$

with temperature T. For a better comparison *Fick's second law of diffusion* is written here again, with Henry's law (4) already applied to substitute the concentration c by the pressure p:

$$\frac{\partial p}{\partial t} = \frac{DS}{S} \nabla^2 p \tag{6}$$

Comparing both equations (5), (6) leads to the analogies as collected in table 3. Using the analogy, a thermal analysis is set up to represent a gas diffusion set-up. Gas pressures for the diffusion process (4) are applied in the framework of temperatures and therefore called pseudo-temperature hereafter. The material's diffusion coefficient is linked to the thermal conductivity. At the left and right boundary of the domain the pseudo-temperature is set to ambient pressure. Zero thermal gas flux is prescribed at the top and bottom boundary because the gas must not penetrate these boundaries.

A structural-thermal analysis can be run in MSC Marc and calculates the results. This is a big advantage, as two Marc-inherent solving capabilities can be used. No additional code has to be written for this purpose. However, to avoid non-physical effects, any influence from the temperature on the mechanical model has to be disabled. To that end, the coefficient of thermal expansion and the dependency of Young's modulus on the temperature are set to zero.

The mechanical pressure has to be linked with the pseudo-temperature around the pores. As temperature and mechanical pressure are two different, but necessary quantities in the FEA, a parallel approach is chosen. On the one hand, to calculate the mechanically induced change of pressure Δp_{mech} due to change of volume ΔV in the pore. On the other hand, to obtain the diffusion-induced change Δp_{diff} from the thermal solver. Assuming isothermal compression, ideal gas law is applied to determine the pressure in a pore for the next

Table 2: Quantities and values used in the numerical simulations

Quantity	Symbol	Value	Unit
Young's modulus	E	5	MPa
Poisson's ratio	ν	0.35	
Diffusion coefficient of the bulk material	D_{bulk}	$5 \cdot 10^{-12}$	m^2/s
Solubility in bulk material	S_{s}	$4.2 \cdot 10^{-4}$	$\mathrm{mol/Pa/m}^3$
Solubility ratio	S_{s}/RT	1	
Ambient pressure	p_{amb}	10^5	Pa
Pressure load	p_{load}	15, 20	p_{amb}
Porosity	ϕ	$0.15 \ldots 0.6$	
Width	w	100	mm
Height	h	100	mm
Time step	Δt	$1 \ldots 31$	days
Number of time steps	n_{ts}	$100 \ldots 200$	
Number of elements	n_{elem}	$100\,000 \ldots 200\,000$	
Number of pores	n_{pore}	200	

time step t^{i+1}

$$\begin{aligned} p^{i+1} &= p^i + \Delta p^i_{\text{diff}} + \Delta p^i_{\text{mech}} \\ &= p^i + \Delta p^i_{\text{diff}} + \Delta V^i \cdot \tfrac{p^i}{V^i}. \end{aligned} \tag{7}$$

Based on this idea, a Python script is written to set up and control a diffusion analysis in MSC Marc. Figure 4 illustrates the algorithm chosen to perform the simulation. The simulation starts by *loading and meshing a geometry*. The *material is defined* as pure elastic with a mass density of $\rho = 0$ to avoid dynamical effects. For the thermal properties of the material the specific heat capacity is set $\rho_{\text{therm}} c_{\text{p}} = S_{\text{s}}$, too. The thermal conductivity is set to the product of the diffusion coefficient and gas solubility of the bulk material $k = DS_{\text{s}}$ (see table 3).

Next, the *boundary and initial conditions* for mechanical stress, strain and pseudo-temperature are set and one time step is simulated. Now, the new gas pressure inside each pore is calculated with equation (7) taking into account the results from the mechanical and thermal simulation.

Since the pores are not material, they are not captured by the meshing, thereby allowing the application of a mechanical pressure on the boundaries of the pores as needed for the simulation. Thus, one supplementary artificial element for each pore is generated to account for the material of the gas. It models the energy content of the respective pore in the thermal solver. From the comparison made between thermal conduction and mass diffusion (table 3) the artificial volume V_{art} of the supplementary element equals $V_{\text{art}} S_{\text{s}} = V_{\text{pore}} RT$. Therefore, the specific heat capacity of the supplementary element's material is set $c_{\text{p}} = V_{\text{pore}}/V_{\text{art}} \cdot RT/S_{\text{s}}$. By linking the supplementary element with the boundary of the respective pore, the correct initial condition for the pseudo-temperature can be imposed. However, mechanical pressures at the interface of the pores can only be applied in the form of boundary conditions, which is not possible during run-time with MSC Marc. For this reason, the simulation has to be halted after one time step to update the boundary conditions. Nodal displacement and pseudo-temperature are transferred to the next time step by the help of initial conditions.

Table 3: Comparison of the heat equation with Fick's second law

	Thermal conduction		Mass diffusion
PDE	$\partial_t T = (k/\rho c_{\text{p}}) \nabla^2 T$		$S \partial_t p = DS \nabla^2 p$
	T	$\leftrightarrow$	p
	k	$\leftrightarrow$	DS
	ρc_{p}	$\leftrightarrow$	S
Storage	$Q = \int V c_{\text{p}} dT$		$E = \int V \cdot RT/S_{\text{s}} dp$
in pore	$V c_{\text{p}}$	$\leftrightarrow$	$V \cdot RT/S_{\text{s}}$

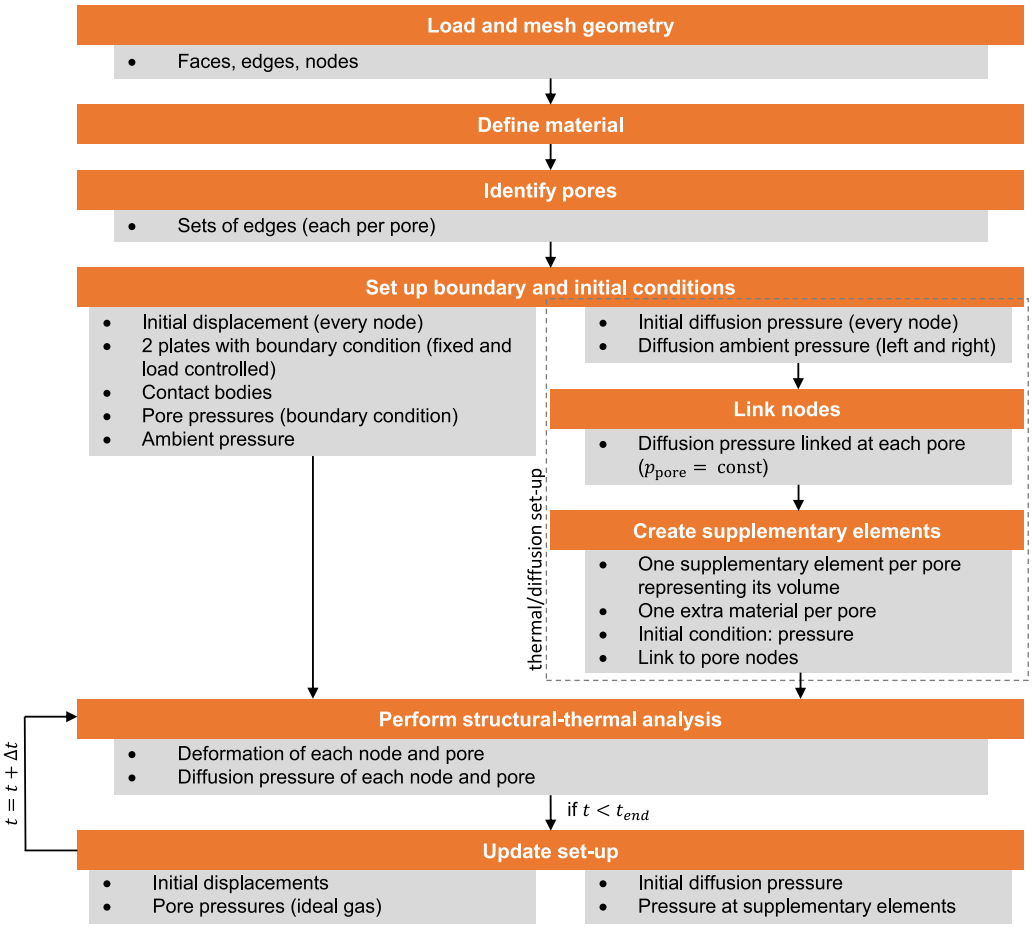

Figure 4: Flow chart: Main steps for a diffusion process simulation using a structural-thermal FEA

With this framework, the *structural-thermal analysis* can be run. The simulated process can be divided into two phases. In the first ten time steps a rather short time step of 10 s is chosen to simulate the yielding due to the mechanical load properly. In this short time, gas diffusion is negligible. After these first steps the time step is increased, so that diffusion effects can be observed.

2.4. Post-Processing

The numerical results are analysed to obtain characteristic values, e. g. characteristic time scales and an effective diffusion coefficient. The results of the simulation are values of pressure at the nodes of the meshed model and in the pores. For an efficient post-processing of the data, the local pressures at the nodes of the unstructured mesh are interpolated to an equidistant, Cartesian mesh. Based on this data, a one-dimensional pressure distribution along the x-direction is obtained by averaging over the y-direction. As the gas cannot diffuse through the top and bottom side of the model, the diffusion in x-direction is the representative one for this process. Relaxation processes lead to a homogenisation of the pressure distribution

in y-direction. It justifies the use of a one-dimensional model for the post-processing, as effective values for the whole structure are of special interest here. Figure 5 shows the contour plot and the corresponding one-dimensional gas-pressure distribution at two different times for a model with 54.4 % porosity and 200 pores. Since the random distribution of pores results is partially imbalanced in vertical direction also the initial amount of gas shows a vertical gradient. This gradient is still present in figure 5 after 6 months.

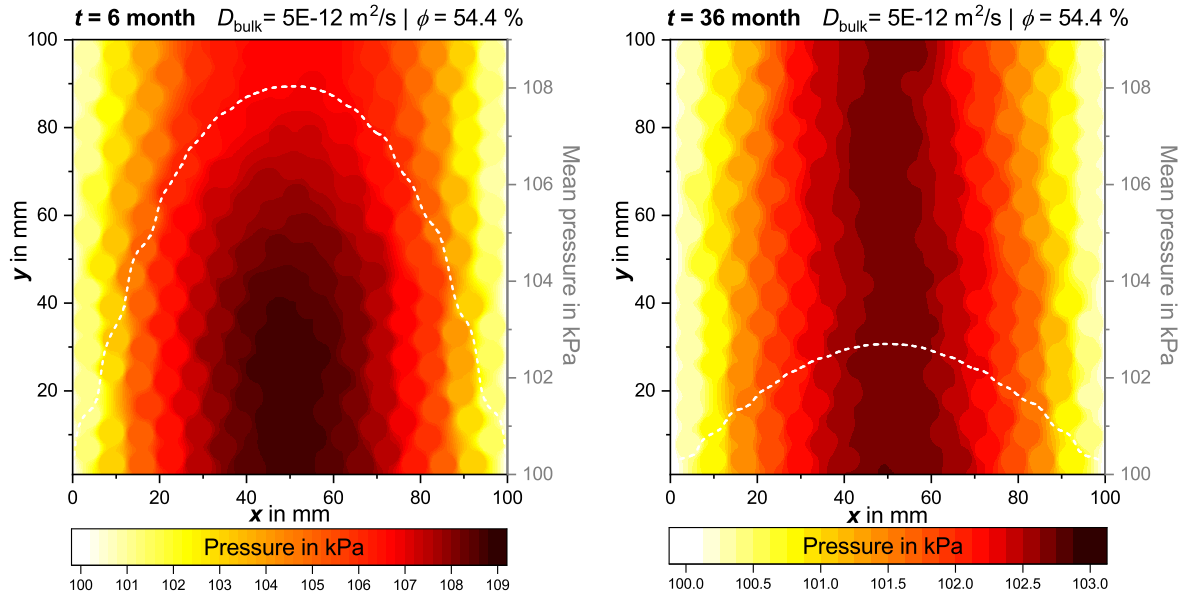

Figure 5: One-dimensional gas-pressure distribution and contours plots of the gas pressure in a two-dimensional porous material (100 mm x 100 mm, 200 pores, $\phi = 54.4\,\%$, $D_{\text{bulk}} = 5$ E-12 $\frac{\text{m}^2}{\text{s}}$) after: 6 month (left) and 36 months (right)

This one-dimensional pressure distribution is derived for each time step. The set of these pressure distributions is used to derive characteristic scalars for the diffusion process. A general solution of the diffusion equation (6) for homogeneous material is the series of exponentially decaying harmonic functions

$$p(x,t) = \sum_{n=1}^{\infty} \tilde{A}_n \sin\left(\frac{\pi n}{2w}x\right) \exp\left(-D_n\left(\frac{\pi n}{2w}\right)^2 t\right) + p_{\text{amb}} \tag{8}$$

in which $\tilde{A}_n$ is a constant amplitude and D_n the effective diffusion coefficient. The curves of the one-dimensional pressure distribution are well presented by *one* sine-function after a short relaxation time. For this reason, coefficients of higher frequency can be neglected as they give only small distribution. Therefore, the period L of the sine-function in (8) has to equal two widths $2w$. From this condition, the relevant sine-function or index n can be determined

$$L = 2\pi / \frac{n\pi}{2w} \stackrel{!}{=} 2w \Rightarrow n = 2.$$

The evolution of the second coefficient is relevant for the calculation of an effective diffusion coefficient D_{eff}. Performing a *fast Fourier transform* (FFT) in space for each time step of the one-dimensional pressure

distribution leads to the values of

$$A_2(t) = \tilde{A}_2 \exp\left(-D_{\text{eff}} \left(\frac{2\pi}{2w}\right)^2 t\right). \tag{9}$$

The argument of the exponential function $\left(-D_{\text{eff}} \left(2\pi/2w\right)^2 t\right)$ in (9) is obtained by fitting the Fourier coefficients in time to an exponential function

$$A_2(t) = \tilde{A}_2 \exp\left(-\frac{t}{\tau_{\text{eff}}}\right) \tag{10}$$

as illustrated in figure 6. Using the characteristic time τ_{eff} of this exponential function, the effective diffusion

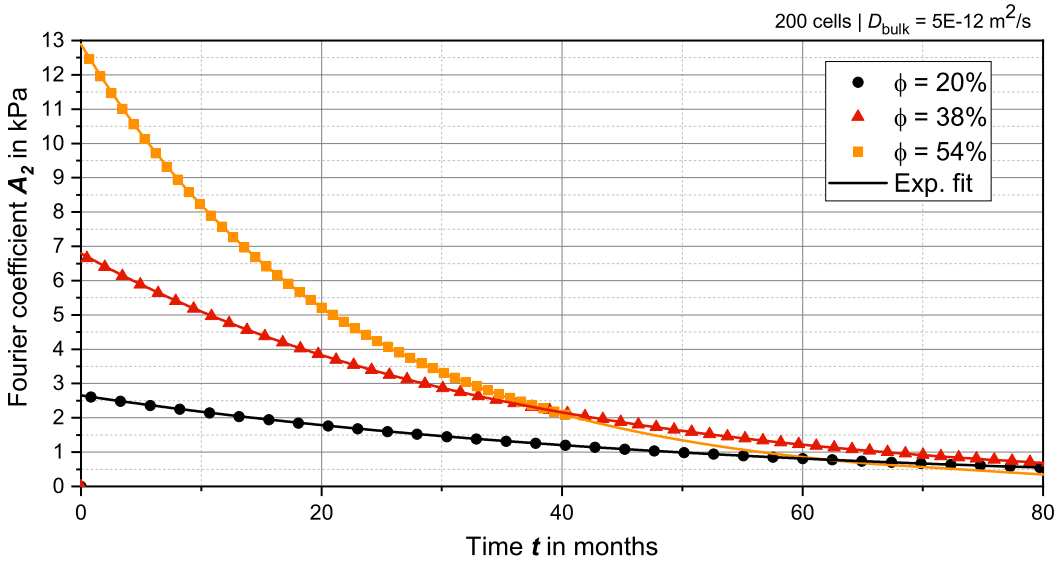

Figure 6: Fourier coefficients $A_2(t)$ (9) for three models with different porosity ϕ = 20, 38, 54 % in time with exponential fit (10) to an exponentially decaying function. Fit parameters: $\tilde{A}_2$ = 2.6538, 6.7925, 12.8915 kPa; τ_{eff} = 50.6930, 34.8971, 22.1224 month.

coefficient D_{eff} for the simulated porous material is derived by

$$D_{\text{eff}} = \frac{w^2}{\tau_{\text{eff}} \pi^2}. \tag{11}$$

In some cases, the pressure cannot be fitted well to a sine-function, e. g. for inhomogeneously distributed pores. To derive a characteristic time nonetheless, another approach is chosen. A characteristic diffusion time scale τ_{diff} can be derived from the decay of pressure. For this purpose, the pressure distribution is averaged in each time step over the porous material including pores and solid material, resulting in a *mean pressure* $\bar{p}(t)$. This mean pressure shows an exponentially decaying behaviour in time. Fitting it to such an exponential function

$$\bar{p}(t) = p_0 \cdot \exp\left(-\frac{t}{\tau_{\text{diff}}}\right) \tag{12}$$

leads to the characteristic time τ_{diff}. Similarly, a time scale τ_{pore} can be defined taking into account only the pressure inside all pores to derive the mean pressure $\bar{p}_{\text{pore}}$.

2.5. Grid study

In order to assess the influence of spatial resolution, a convergence study on the mesh is conducted. For this purpose, a simulation is performed using three different resolutions (a, b, c) with increasing numbers of elements. Figure 7 shows sections of the discretized geometries.

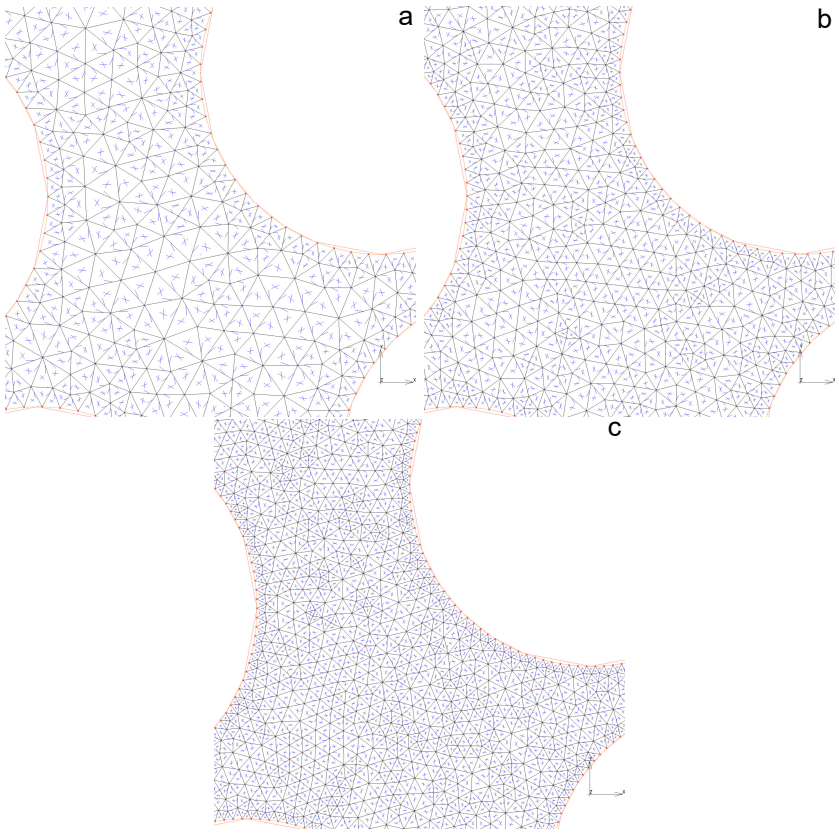

Figure 7: Section of the discretized mesh for a geometry with 200 randomly distributed pores with a porosity of $\phi = 45\,\%$. Three different discretisations (a, b, c) with $n_{\text{elem}} = 100\,000,\ 200\,000,\ 400\,000$.

Figure 8 shows the mean pressure evolution $\bar{p}(t)$ on a geometry with 200 randomly distributed pores and a porosity of $\phi = 45\,\%$ for three different meshes with $n_{\text{elem}} = 100\,000,\ 200\,000,\ 400\,000$ elements, respectively. The relative deviation between two configurations α and β is calculated by

$$\Delta_{\alpha,\beta} = \sum \left(\frac{\sqrt{(\bar{p}_\alpha - \bar{p}_\beta)^2}}{\bar{p}_\beta - p_{\text{amb}}} \right) / n_{\text{ts}}. \tag{13}$$

Herein $\bar{p}$ denotes the mean pressure averaged over the whole domain at a certain time step and $\sum$ symbolizes the sum over all time steps. The results on these meshes show minor deviations up to $\Delta_{a,c} = 7\,\%$ and

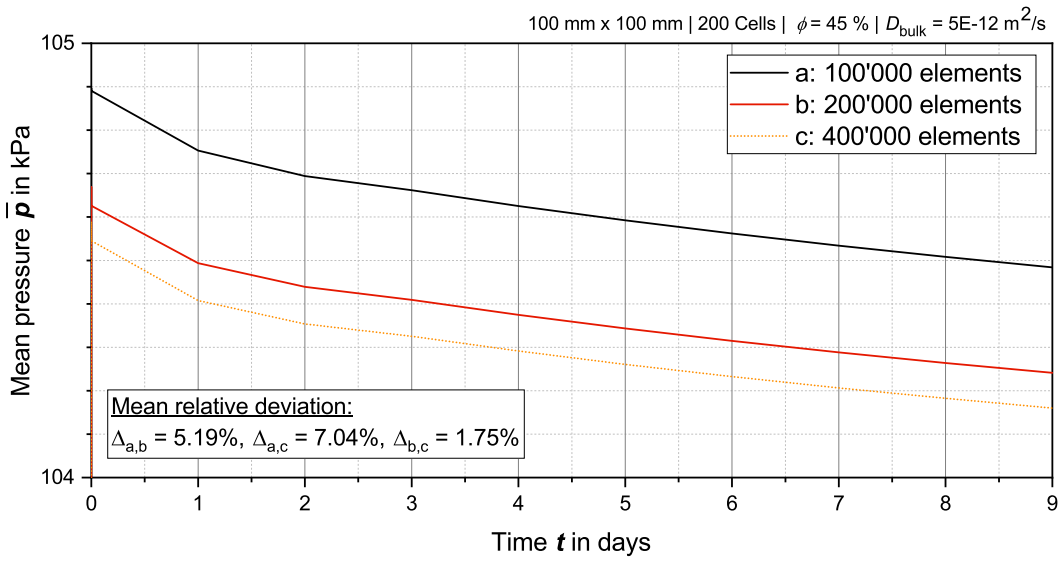

Figure 8: Convergence study on a mesh for a model of 200 randomly distributed pores with a porosity of $\phi = 45\,\%$. Mean pressure curves for three different discretisations (a, b, c) with $n_{\text{elem}} = 100\,000,\ 200\,000,\ 400\,000$. Relative deviations according to (13).

converge. As the extensive additional cost for the finer discretisation is not justified by this difference, the coarsest element size (a) has been used for this work.

A convergence study in time is conducted as well. Figure 9 shows the mean pressure evolution $\bar{p}(t)$ on a geometry with 200 randomly distributed pores and a porosity of $\phi = 50\,\%$ for three different lengths of the time step with $\Delta t = 7,\ 15,\ 30\,\text{d}$, respectively. Interpolating the results to the time steps of the simulation with the coarser time discretisation, equation (13) is used to calculate the mean deviation. It shows that the influence of the chosen time step is below 0.1 % on the mean pressure.

3. Results

In the first step, simulations of diffusion through a porous material under load are performed on two-dimensional domains ($w = h = 100\,\text{mm}$) with either 200 randomly distributed pores or with 25 to 225 pores, arranged equidistantly on a Cartesian lattice.

The *one-dimensional pressure* curves of all simulations show a characteristic sinusoidal profile after a short relaxation time. This demonstrates that the results agree to the Fickian diffusion model. Thus, the effective material approach according to equation (8) can be applied to determine effective properties.

Figure 10 shows the *relative effective diffusion coefficients* $D_{\text{eff}}/D_{\text{bulk}}$ obtained from equation (11). The diffusion coefficient increases with increasing porosity. It meets the expectation that an increasing amount of bulk material constitutes increasing diffusion resistance. The data suggest a possible exponential relation

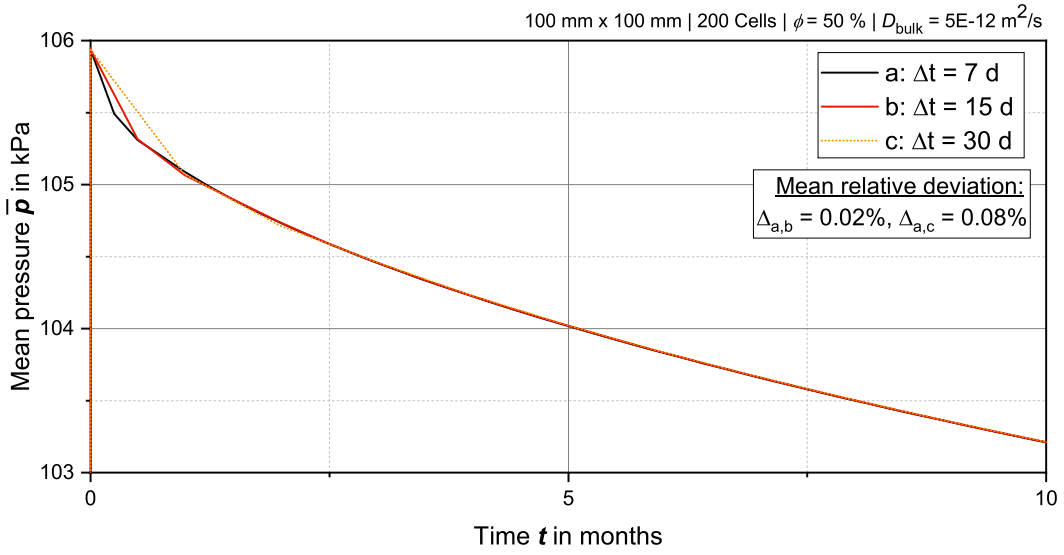

Figure 9: Convergence study in time for a model of 200 randomly distributed pores with a porosity of $\phi = 50\,\%$. Mean pressure curves for three different time steps (a, b, c) with $\Delta t = 7,\ 15,\ 30\,\mathrm{d}$. Relative deviations according to (13).

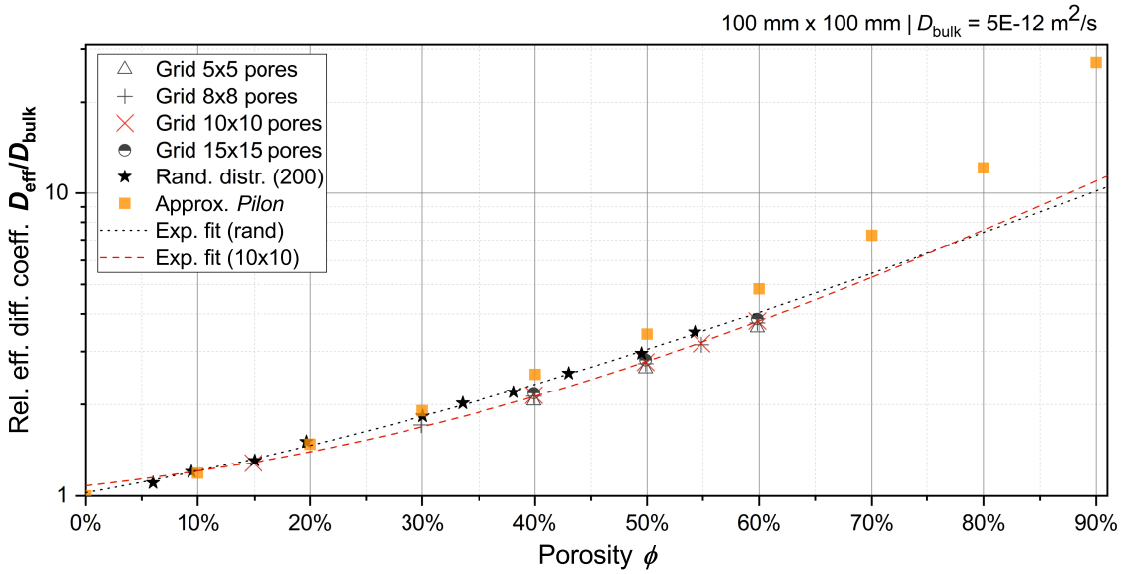

Figure 10: Relative effective diffusion coefficients $D_{\mathrm{eff}}/D_{\mathrm{bulk}}$ for different porosities ϕ from simulations on domains with grid-arranged and randomly distributed pores. Analytical values from an approximation by Pilon [6] and exponential fits (14).

between diffusion coefficient and porosity. An exponential fit

$$\frac{D(\phi)}{D_{\mathrm{bulk}}} = D_o + D_1 \exp\left(\frac{\phi}{\phi_1}\right), \quad \begin{cases} D_o = 0.5663,\ D_1 = 0.4589,\ \phi_1 = 29.60\% & \text{random} \\ D_o = 0.8289,\ D_1 = 0.2511,\ \phi_1 = 24.34\% & \text{10x10} \end{cases} \tag{14}$$

is shown in figure 10. For a porosity of $\phi = 0$, equation (14) yields

$$D_{\mathrm{eff}}/D_{\mathrm{bulk}} = \begin{cases} 1.0252 & \text{random} \\ 1.08 & \text{10x10} \end{cases},$$

values close to the theoretical result of 1. This again demonstrates the validity of the method. Besides of its quantitative meaning, the effective diffusion coefficient describes the rate of diffusion through the material. It can be used to compare materials with different topologies or porosities. Figure 11 shows, how the resulting D_{eff} relies on the number of pores in the computational domain. Already a small amount of 25 pores gives a reasonable estimate of the effective material properties. However, D_{eff} still rises by 7 % if the number of pores is increased. Above 100 pores, the variation is below 2 %, proving the effective material behaviour of the material.

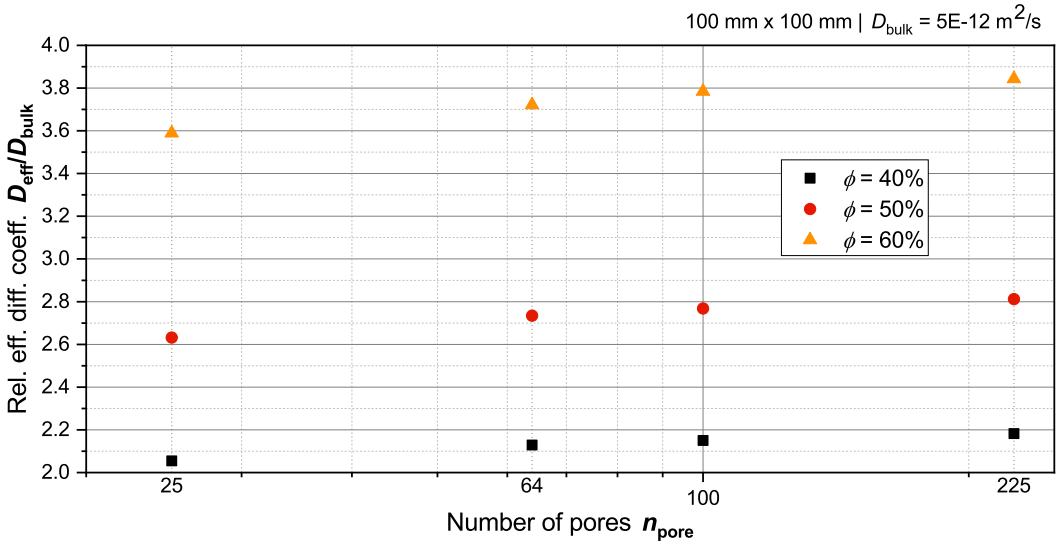

Figure 11: Relative effective diffusion coefficients $D_{\mathrm{eff}}/D_{\mathrm{bulk}}$ for certain numbers of pores n_{pore} from simulations on materials with grid-arranged pores

For large domains or computationally demanding micro-structures, the simulation of long physical times might not be feasible. In that case, simulations of only a few time steps and extrapolation would be beneficial. Figure 12 reports on the relative deviation of the effective diffusion coefficient when the simulation is stopped after a certain fraction of τ_{diff}. To that end, materials with 200 randomly distributed pores at 30 %, 38 %, and 54 % gas fraction, respectively, have been simulated and post-processed, taking only a certain fraction of the simulated time into account. Already after 50 % of τ_{diff}, the resulting effective diffusion coefficients show deviations smaller than 0.5 %.

Averaging the pressure in all pores at a given instant yields the mean pore pressure $\bar{p}_{\mathrm{pore}}$. Figure 13 shows its evolution over time for simulations with different porosities, presented in figure 10 as well. The

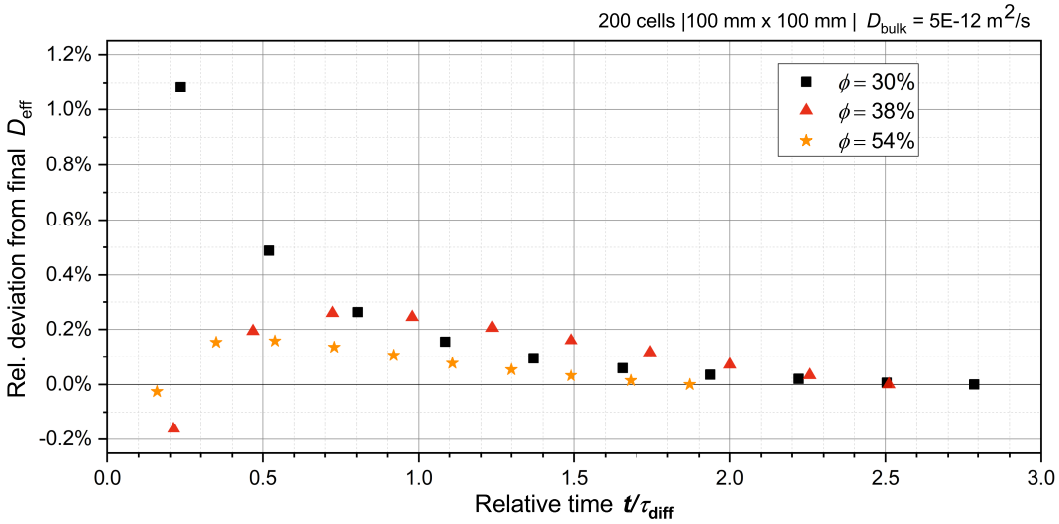

Figure 12: Deviation of the effective diffusion coefficient after certain times from final value after all increments. For three models with 200 randomly distributed pores and porosities of $\phi = 30,\ 38,\ 54\,\%$. Total number of time steps $n_{\mathrm{ts}} = 180$, time step $\Delta t = 20,\ 15,\ 7$ d.

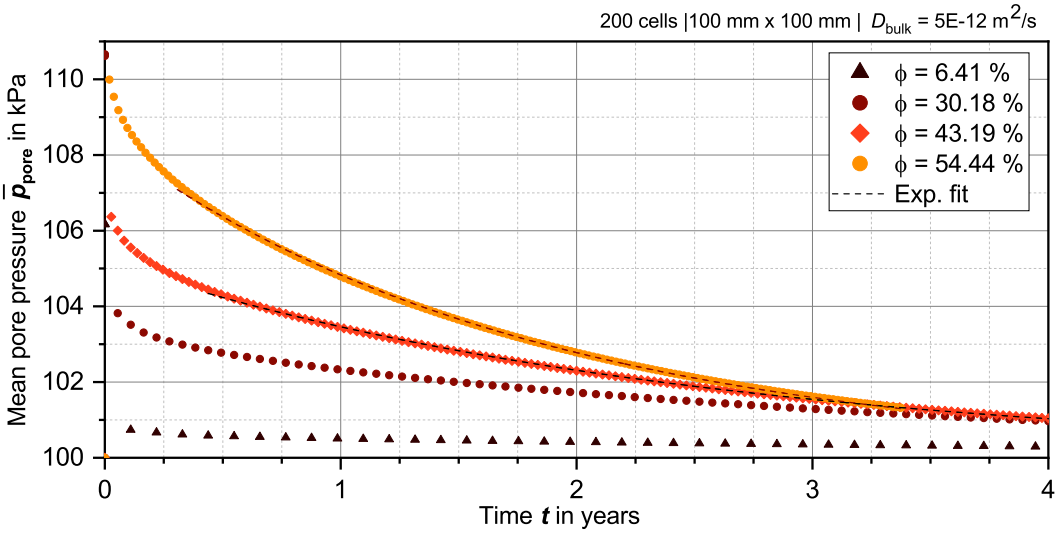

Figure 13: Mean pore pressure evolution in time $p(t)$ for materials with 200 randomly distributed pores and different porosities. Exponential fits after 20 time steps (15) for $\phi = 54.4\,\%,\ 43.2\,\%$ with $p_{\mathrm{amb}} = 100\,\mathrm{kPa}$; $p_1 = 8.399,\ 5.183\,\mathrm{kPa}$; $\tau_{\mathrm{pore}} = 1.808,\ 2.477\,\mathrm{a}$.

mean pore pressure decays approximately exponentially in time, which is in line with experimental findings [16].

The characteristic decay times τ_{pore} are obtained from fitting the mean pore pressure $\bar{p}_{\mathrm{pore}}(t)$ evolution to an exponential function

$$\bar{p}_{\mathrm{pore}}(t) = p_{\mathrm{amb}} + p_1 \exp\left(-t/\tau_{\mathrm{pore}}\right) \tag{15}$$

starting after a certain number of time steps. Figure 14 demonstrates the drop of τ_{pore} with increasing porosity. The graph suggests a linear relation in the investigated porosity range

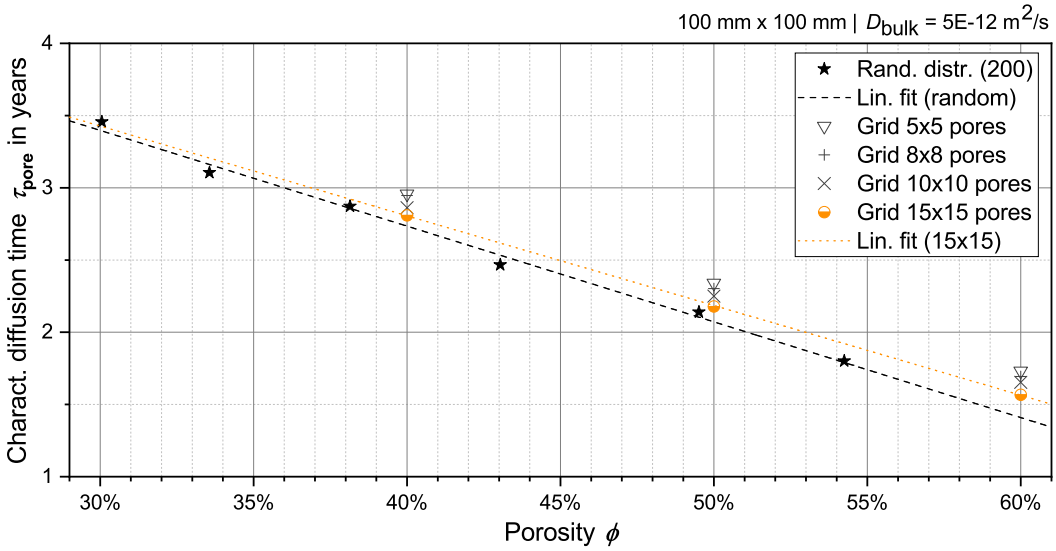

Figure 14: Characteristic diffusion time τ_{pore} from pore pressures for models with 200 randomly distributed pores and with grid-arranged pores as function of the porosity ϕ. Including linear fits given in equation (16).

$$\tau_{\text{pore}} = \tau_o - \tau_1 \cdot \phi, \quad \begin{cases} \tau_o = 5.386\,\text{a},\ \tau_1 = 0.06628\,\text{a}/\% & \text{random} \\ \tau_o = 5.291\,\text{a},\ \tau_1 = 0.06212\,\text{a}/\% & \text{15x15} \end{cases} \tag{16}$$

Figure 14 shows a slight decrease of τ_{pore} for an increasing number of pores in case of material with grid-arranged pores. This might be due to more homogeneous and thus, more efficient distribution of gas flux. However, no significant qualitative change of behaviour is detected. Therefore, the consideration of the structure as an effective material seems legitimate for the deployed number of cells.

After measuring the influence of porosity, now the influence of pore shape is considered. To that end, four additional simulations are conducted using randomly distributed *elliptical pores*. The ratio of the semi axes of all pores is set either to 0.5 or to 2, yielding horizontally or vertically oriented ellipses, respectively. Figure 15 shows the relative effective diffusion coefficients $D_{\text{eff}}/D_{\text{bulk}}$ for domains with circular pores compared to ones with horizontally or vertically elongated pores at two different levels of porosity ϕ.

This bar chart suggest significantly faster diffusion for domains with horizontally arranged pores than for vertically arranged ones or for domains for circular pores. The difference in the diffusion coefficient between the latter ones are small. The figure shows a slight decrease in the diffusion coefficient if the pores are elliptical and vertically arranged, and not circular. In interpreting this tendency, one should, however, be cautious. The pore centers do not coincide. Thus, randomly occurring lines of pores may bias this result. Nonetheless, one could carefully venture a first explanation: The horizontal alignment of the pores,

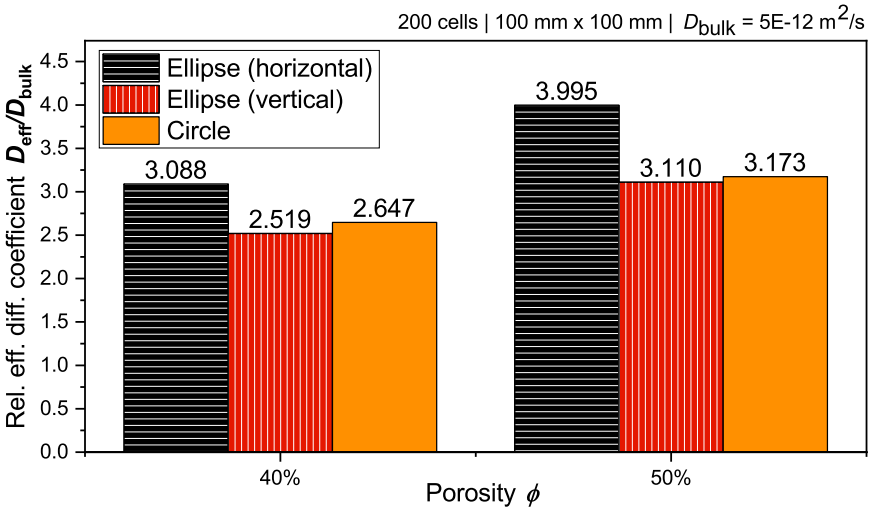

Figure 15: Comparison of relative effective diffusion coefficients of structures with horizontally aligned elliptical pores, vertically aligned elliptical pores and with 200 randomly distributed, circular pores. ($\phi = 40,\ 50\,\%$)

i. e. alignment in the direction of the diffusion, may enable the gas to diffuse through less bulk material in 'choosing' its way through the pores. This could accelerate the diffusion since the gas is considered to diffuse through the pores instantaneously, whereas the diffusion through the solid is slow. By this, the slower diffusion in case of vertically orientated, elliptical cells could be explained as well. In that case the gas might be forced to diffuse through effectively more bulk material.

In a third step, the influence of inhomogeneous pore distribution is investigated. To that end, the pores are arranged on a Cartesian lattice and shifted horizontally, leaving either a band of solid material of size $\lambda \cdot w$ in the middle, or leaving a band of size $\lambda/2 \cdot w$ at both sides (see figure 16). This is done for a constant overall porosity of $\phi = 40\,\%$ and constant dimension of the material $w = h = 100\,\mathrm{mm}$, to investigate the influence of this *shifting*. Due to the inhomogeneous distribution sinusoidal ansatz functions according to equation (8) do not represent the gas distribution. Consequently, characteristic times of exponential decay according to equation (12) are employed here. The characteristic diffusion time τ_{diff} for different widths of the shifting λ are presented in figure 16. The diffusive decay for accumulation of solid material on the outside is slower than for accumulation in the middle of the material. In case of positive shift, the diffusion time is well represented by a linear function

$$\tau_{\mathrm{diff}} = 2.958\,\mathrm{a} + 0.04352\,\frac{\mathrm{a}}{\%} \cdot \lambda. \tag{17}$$

The slope of the linear fit corresponds to the constitution of an additional diffusion barrier with growing thickness.

In case of negative shift, two effects have to be considered here. Firstly, the gas diffusion within the bubble cluster increases because of decreasing wall thickness between the bubbles. Secondly, the bubbles are

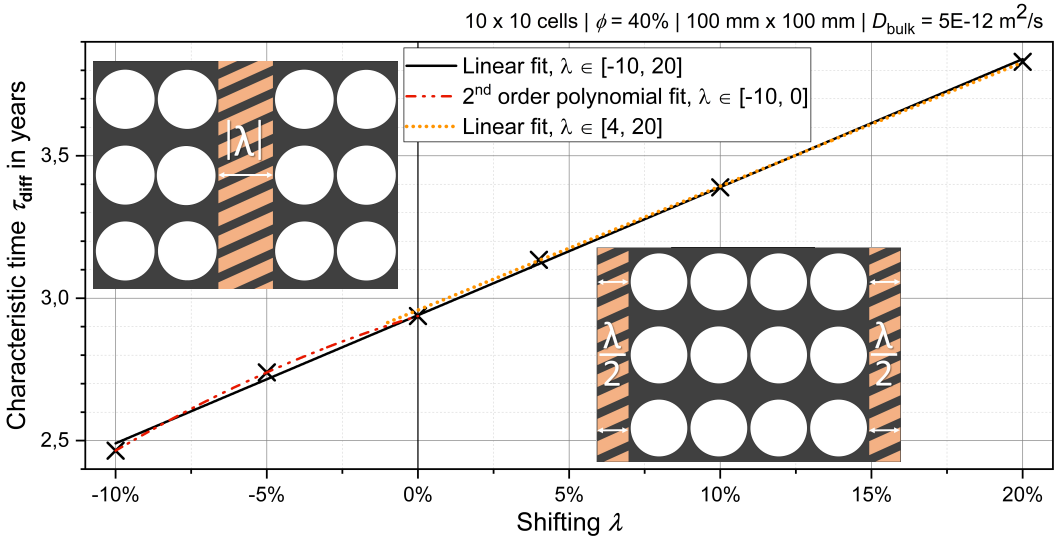

Figure 16: Characteristic diffusion time τ_{diff} for structures with 10x10 grid-aligned circular pores for different shifting. Negative λ: Space in the middle. Positive λ: Space at the sides.

shifted towards the sides, so the contained gas has to cover smaller diffusion lengths to reach the outside. The combination of both effects results in a nonlinear decrease of the diffusion time with increasing shifting. In this case, the diffusion time might by estimated by a second order polynomial function

$$\tau_{\mathrm{diff}} = 2.938\,\mathrm{a} + 0.03200\,\mathrm{a}\frac{\lambda}{\%} \cdot -0.00153\,\mathrm{a}\left(\frac{\lambda}{\%}\right)^2 . \tag{18}$$

Interestingly, the positive and the negative shifting results in a comparable slope at zero shifting and a continuous and smooth curve. A linear fit over the whole simulated range of λ yields

$$\tau_{\mathrm{diff}} = 2.940\,\mathrm{a} + 0.04496\,\mathrm{a}\frac{\lambda}{\%} \cdot . \tag{19}$$

4. Discussion

The method developed to simulate diffusion using a FEA program is successfully implemented in a Python script. The approach to employ the thermal solver proofs to be working. A stable code is developed and leads to quantitatively plausible results. For the simulation ideal gas law is used and isothermal compression is assumed. In that way, temperature dependencies are neglected. This is reasonable for long-term relaxation processes in polymer foam construction parts. However, in case of fast diffusion, e. g. for hydrogen storage in foams, thermal effects should be considered.

As the diffusion coefficient is set to a constant value, its dependency on the concentration and local mechanical stress is neglected. It would be difficult to implement the latter, because there is no direct

interaction between diffusive flux and mechanical stress during a time step. The interaction is implemented by synchronizing initial and boundary conditions between the time steps. However, if the time steps are short enough, the results converge as demonstrated by the convergence study. Due to this parallel approach, the FEA program must stop after each time step and needs to be updated. Consequently, the simulation requires rather long computation times to perform. Nevertheless, it could be demonstrated that reliable diffusion coefficients can be determined by simulating only 0.5 diffusive time scales and thereby reducing the computational effort significantly (see figure 12).

The diffusion through the pores is considered to be taking place instantaneously, as the pore pressure is set to a constant value. In case of single component gases, the pressure equalises inside a pore with the speed of sound. And also, in case of gas mixtures the approach is reasonable because diffusion coefficients in gas are approximately seven orders of magnitude [17] higher than for diffusion in polymers. Consequently, considering homogeneous conditions inside each pore is reasonable.

The influence of the solubility was neglected by setting its ratio $S_s/S_{\mathrm{gas}} = S_{\mathrm{s}}/RT$ to the value of 1. Smaller solubility in the solid material would reduce the gas flux and thus, decrease the effective diffusion coefficient. Depending on the type of gas and solid, the chosen solubility ratio is in the range of realistic values [3]. Note that here diffusion within the void is not the rate-determining step in the permeation process, and the chosen ratio value of 1 is consistent with previous studies [6] showing no influence of the solubility of the gas in the condensed phase on the effective diffusion coefficient.

Compared to realistic foam, the present simulation is restricted to two dimensions, purely elastic material, spherical or elliptical pores, and the absence of struts, open pores, or other imperfections. This work considers only diffusion of a single gas. In case of mixtures of gases with different diffusion coefficients more complex processes such as demixing or diffusion from ambient gases into the void material could take place. Still, the results show reasonable agreement to experimental investigations of gas diffusion in porous media [3]. The results also show the same magnitudes and tendency in the effective diffusion coefficient as the model developed by Pilon et al. [6] (figure 10).

The program is used to *predict effective diffusion coefficients*. Offering a tool, that can determine a diffusion coefficient without complex, long and expensive experiments is of significant value. Since it computes the distribution of the gas, it could also determine effective positions for probes in experimental investigations, yielding highest sensitivity. However, for the simulations done so far, the pores are considered spherical, limiting the porosity geometrically to $\phi = 91\,\%$ in two dimensions and $\phi = 74\,\%$ in three dimensions. Due to the decreasing wall thickness for increasing porosity, the geometry must be meshed finer, resulting in increasing numbers of elements and high computational effort. In the present study, porosity is limited to $\phi = 60\,\%$. For higher porosities, the initial solid foam structure should be computed considering the generation process of foams [18] or surface evolver simulations [19].

Usually, two-dimensional resolution is instructive about the tendency observed in the principal directions

of three dimensional configurations. For more realistic results pure elastic material behaviour could be replaces by viscoelastic one to simulate creep-experiments. Also, expansion to larger, non-square models with higher porosity could be part of further improvement. Transferring the method into three dimensions is easily possible, because the thermal and the structural solver of many FE programs are implemented in three dimensions as well. Future research could use the programs ability to simulate set-ups with time-dependent boundary conditions and complex geometries, making use of the universal character of the approach.

For the simulated geometries and a porosity ranging from 30 % to 60 %, a nearly linear correlation between characteristic diffusion time and porosity can be observed (figure 14). Quick estimations about the time scale for a certain model can be made with equation (16). Subsequently, significant influence of the pore shape (figure 15) and pore distribution (figure 16) have been identified. In the considered parameter range, variations up to 30 % on the diffusion rate are to be observed.

Regarding the results, one can state, that diffusion is a non-negligible factor for long-time loaded solid closed-cell porous materials; though strongly depending on the material, the dimension of the model, its porosity and the gas chosen. For the structures simulated a major change in pore pressure caused by diffusion acts on the time scale of the order of months or few years.

Summarising, one can say that a tool is created that can handle complex loadings, cyclical deformation and other loads, limited only by the computer power to handle fine meshes. It can be used for manifold set-ups and may help for the design of porous materials such as polymer foam. Using simplifying assumptions like presence of a single gas, constant solubility and isothermal state, it simulates the pressure, respectively concentration, change inside the material. In that way, it offers *insight into the diffusion process* going on and allows to derive effective diffusion coefficients.

Competing interest. The authors declare that they have no competing financial interest.

References

[1] L. J. Gibson, M. F. Ashby, Cellular Solids: Structure and Properties, 2nd Edition, Cambridge University Press, Cambridge, 1997. doi:10.1017/cbo9781139878326.
URL https://www.cambridge.org/core/books/cellular-solids/BC25789552BAA8E3CAD5E1D105612AB5

[2] R. Bouix, V. Philippe, J.-L. Lataillade, Polypropylene foam behaviour under dynamic loadings: Strain rate, density and microstructure effects, International Journal of Impact Engineering 36 (2009) 329–342. doi:10.1016/j.ijimpeng.2007.11.007.

[3] S. Alsoy, Modeling of diffusion in closed cell polymeric foams, Journal of Cellular Plastics 35 (3) (1999) 247–271.
URL http://journals.sagepub.com/doi/pdf/10.1177/0021955X9903500305

[4] B. Song, W. W. Chen, S. Dou, N. A. Winfree, J. H. Kang, Strain-rate effects on elastic and early cell-collapse responses of a polystyrene foam, International Journal of Impact Engineering 31 (5) (2005) 509 – 521. doi:https://doi.org/10.1016/j.ijimpeng.2004.02.003.
URL http://www.sciencedirect.com/science/article/pii/S0734743X04000314

[5] S. Lequin, D. Chassagne, T. Karbowiak, J.-M. Simon, C. Paulin, J.-P. Bellat, Diffusion of oxygen in cork, J. Agric. Food Chem. 60 (13) (2012) 3348–3356. doi:10.1021/jf204655c.
URL https://doi.org/10.1021/jf204655c

[6] L. Pilon, A. G. Fedorov, R. Viskanta, Gas diffusion in closed-cell foams, Journal of Cellular Plastics 36 (2000) 451–474. doi:10.1106/v8xj-yfpq-lgl6-qvfm.

[7] B. J. Briscoe, T. Savvas, Gas diffusion in dense poly(ethylene) foams, Advances in Polymer Technology 17 (2) (1998) 87–106.

[8] D. T. Wadiak, Application of the finite-element method to the diffusion and reaction of chemical species in multilayered polymeric bodies, Mathematical Modelling 7 (2-3) (1986) 385–395.

[9] M. Rodríguez-Pérez, J. Ruiz-Herrero, E. Solórzano, J. De Saja, Gas diffusion in polyolefin foams during creep test. effect on impact behaviour and recovery after creep, Cellular Polymers 25 (4) (2006) 221–236.

[10] M. Rodríguez-Pérez, F. Hidalgo, E. Solórzano, J. de Saja, Measuring the time evolution of the gas pressure in closed cell polyolefin foams produced by compression moulding, Polymer Testing 28 (2) (2009) 188 – 195.

[11] M. Modesti, A. Lorenzetti, C. Dall'Acqua, New experimental method for determination of effective diffusion coefficient of blowing agents in polyurethane foams, Polymer Engineering & Science 44 (12) (2004) 2229–2239. arXiv:https://onlinelibrary.wiley.com/doi/pdf/10.1002/pen.20250, doi:10.1002/pen.20250.
URL https://onlinelibrary.wiley.com/doi/abs/10.1002/pen.20250

[12] M. Svanström, O. Ramnäs, M. Olsson, U. Jarfelt, Determination of effective diffusion coefficients in rigid polyurethane foam, Cellular Polymers 16 (1997) 182–193.

[13] A. Boersma, D. Cangialosi, S. J. Picken, Mobility and solubility of antioxidants and oxygen in glassy polymers. iii. influence of deformation and orientation on oxygen permeability, Polymer 44 (8) (2003) 2463 – 2471. doi:https://doi.org/10.1016/S0032-3861(03)00039-9.
URL http://www.sciencedirect.com/science/article/pii/S0032386103000399

[14] J. Crank, Diffusion in Polymers, Academic Press, New York, 1968, Ch. Methods of measurement, pp. 1–39.

[15] J. Crank, G. S. Park, The Mathematics of Diffusion, Oxford University Press, London, 1975, Ch. Methods of measurement, pp. 1–39.

[16] J. Ruiz-Herrero, M. Rodríguez-Pérez, J. de Saja, Effective diffusion coefficient for the gas contained in closed cell polyethylene-based foams subjected to compressive creep tests, Polymer (Mar. 2005).

[17] E. L. Cussler, Diffusion: Mass Transfer in Fluid Systems, 3rd Edition, Cambridge Series in Chemical Engineering, Cambridge University Press, 2009. doi:10.1017/CBO9780511805134.

[18] I. Dabo, T. Roland, G. Dalongeville, C. Gauthier, P. Kékicheff, Ad-hoc modeling of closed-cell foam microstructures for structure-properties relationships, European Journal of Mechanics - A/Solids 75 (01 2019). doi:10.1016/j.euromechsol.2019.01.016.

[19] K. A. Brakke, The surface evolver, Experimental Mathematics 1 (2) (1992) 141–165. arXiv:https://doi.org/10.1080/10586458.1992.10504253, doi:10.1080/10586458.1992.10504253.
URL https://doi.org/10.1080/10586458.1992.10504253